HEFAT2010
7th International Conference on Heat Transfer, Fluid Mechanics and Thermodynamics
19-21 July 2010
Antalya, Turkey

SHAPE EFFECTS OF HEATERS IN NANOFLUID POOL BOILING

Ranganathan Kumar* and Diane M. Vazquez
*Author for correspondence
Department of Mechanical, Materials and Aerospace Engineering,
University of Central Florida,
Orlando, FL, USA
E-mail: Rnkumar@mail.ucf.edu

ABSTRACT

This paper deals with a study of enhanced critical heat flux (CHF) and burnout heat flux (BHF) in pool boiling of water with suspended silica nanoparticles using Nichrome wires and ribbons. Previously our group and other researchers have reported three-digit percentage increase in critical heat flux in silica nanofluids. This study investigates the effect of various heater surface dimensions and cross-sectional shapes on pool boiling heat transfer characteristics of water and water-based nanofluids. Our data suggest that the CHF and BHF decrease as heater surface area increases. For concentrations from 0.1vol% to 2vol%, various properties such as viscosity, pH, and surface tension as well as silica deposition on surface and glowing length of ribbon are measured in order to study the possible factors in the heat transfer behavior of nanofluids. The deposition of the particles on the wire allows high heat transfer through inter-agglomerate pores, resulting in a nearly 3-fold increase in burnout heat flux at very low concentrations. As the concentration is increased, the CHF and BHF each decrease prior to increasing again at higher concentrations. Results show a maximum of 270% CHF enhancement for ribbon-type heaters. A trend is presented for the effect of concentration on both CHF and BHF, and visualization of boiling experiments aids with determination of bubble sizes, nucleation, and flow regimes.

Keywords - critical heat flux; nanofluid; pool boiling; deposition; concentration

INTRODUCTION

In the regime of nucleate boiling there are two major physical mechanisms that govern the thermal transport: 1) latent heat of vaporization, where superheated liquid is vaporized, carrying away with it heat energy from the surface, and 2) dryout of the heater surface. These two mechanisms work against each other in the overall purpose of effectively carrying heat away from the surface and thus, delaying the critical failure of the heater element in the pool boiling scenario. As the wall superheat is increased in the nucleate boiling regime, the number of active nucleation sites increases and the frequency of the isolated bubbles increases. The spacing between the nucleation sites becomes closer, causing the bubbles to coalesce, and with the bubbles rising so quickly, this creates a column of vapor slugs. In the higher heat flux range of the nucleate boiling regime (the regime of slugs and columns), the amount of vapor produced near the heater increases to such an extent that the liquid is increasingly unable to wet the surface, thus creating the gradual dryout of the surface and the onset of the critical heat flux condition. This is the general concensus in the literature; although, several theories have been postulated for the departure from nucleate boiling (DNB), three of which are summarized below.

The hydrodynamic instability theory [1] postulates that the high velocity of the vapor rising creates an instability with the slower, descending liquid, creating a distorted column of vapor and interrupting the liquid flow to the heater surface. The decreasing amount of liquid that reaches the surface is vaporized, leading to the blanketing of vapor and CHF. Another theory [2] explains that dry spots are formed over hot portions of the surface and are subsequently rewet axially upon bubble departure. DNB occurs when the horizontal force of the vapor is greater than the liquid vapor surface tension, causing the liquid to further receed and finally dry out the surface. Still another theory [3] proposes that at high heat flux a vapor plume or mushroom hovers above the surface, being fed underneath by numerous vapor feeder jets rising from the surface. The feeder jet develops from an individual nucleation site when the rate of vaporization is so high that a continuous jet of vapor rises. A layer of liquid, termed the macrolayer, separates the large vapor bubble from the surface and is trapped in between the feeder jets. DNB is said to occur when this macrolayer is depleted or when the hovering time is greater than the time required to dry out the macrolayer.

Of particular concern in this investigation is the CHF of the heater element which is of great importance to its functional life. This is the heating point at which additional heating

causes a sudden increase in temperature, glowing of the heater element, and eventual burnout of the heater (controlled heat flux case). For the usefulness of a heater in practical application, it is essential to remain well below the critical heat flux. Research studies have shown a CHF enhancement of ~200% for silica nanofluids [4], [5] and ~100% enhancement for titania nanofluids on wire heaters [6]. You et al. [7] reported a ~200% enhancement for alumina on a flat plate, while Bang and Chang [8] found ~32% and ~13% CHF enhancement for alumina on a horizontal and vertical plate, respectively. Thus, these nanofluids have potential applications in electronic cooling, heat exchangers, and optical systems.

Various parameters have been studied to determine the cause of CHF enhancement due to nanoparticles, and studies have shown that the nanoparticle surface coating (deposition) is the main factor in the enhancement of pool boiling CHF in nanofluids [6], [9].

Surface roughness has been shown to increase as a result of the nanoparticle layer on the surface, directly increasing the effective surface area, and this has been shown to enhance boiling performance [10]. However, there are conflicting results in literature [4], [7], [8], [11], [12] regarding the negative or neutral effects of surface roughness on boiling heat transfer, although these showed significant increase in CHF. It seems that surface roughness alone cannot determine the nucleate boiling heat transfer behavior; however, it is certain that changing roughness affects surface characteristics, such as the apparent contact angle [13].

A more important parameter that has been investigated is the contact angle which is affected by the surface roughness. Reduction in three-phase contact angle (increased wettability of a surface) due to nanoparticle-deposited surfaces has been shown to have a positive correlation with enhancement of CHF [5], [11], [14], [15], [16], [17]. Kim et al. [11] report that the contact angle of a water droplet on a nanosilica-boiled surface ranged from 8°-18°, and for 0.1vol% silica nanofluid droplet on nanosilica-coated surface the angle was 21°, both much less than the nominal angle of water on a clean metal surface ~80°.

Kim and Kim [18] proposed that capillary wicking through the porous layer causes the cooler fluid to reach and wet the heater surface, thus delaying the onset of critical condtition due to rewetting of a dry spot in bubble growth. In another study, it is suggested that capillary wicking through the micro-flow-passes creates a thin film of cooler fluid covering the particles, and evaporation of this thin film on the increased effective boiling surface area contributes to the enhanced boiling heat transfer [19].

Nevertheless, Coursey et al. [16] state that an improved surface wettability due to deposition may be negated by another mechanism such as fouling. Therefore, there may be a limit where increasing the nanoparticle concentration above a certain threshold could impose a neutral or detrimental effect on the CHF enhancement. Clearly, more research needs to be done in this area to fully understand the effect of nanofluids in pool boiling.

The objective of this study is to investigate the effect of various heater surface dimensions and cross-sectional shapes on pool boiling heat transfer characteristics of water and water-based nanofluids at different concentrations.

EXPERIMENTAL PROCEDURE

Experimental Setup

Even The experimental setup as shown in Figure 1 consists of 30 Amp DC power supply (Kenwood, PD 18-30AD), heater plate (Fisher Scientific), Pyrex glass cylindrical test section, 10mm-thick acrylic cover, coiled double jacketed condenser, multimeter (Agilent, 34401A), data acquisition system (DAQ), and type K thermocouple. Similar to our previous work [20], the experimental procedure involves passing current through a Nichrome wire/ribbon, which serves as the heater element and a temperature sensor simultaneously. Soldered to the Nichrome metal are copper lead wires and voltage sense wires leading to a multimeter. The current work uses a Nichrome ribbon which is oriented horizontally as shown in the inset of Figure 1. The heater circuit assembly is submerged in a pool of approximately 200 mL of sample fluid in the glass test section and is subsequently heated on the plate to the saturation temperature T_{sat} (100°C) at atmospheric pressure, with bulk temperature monitored by the thermocouple. The current is regulated through the DAQ system in this experiment for constant heat flux control, with an initial value of 0.2A (minimal current not affecting wire heating), and it is increased at 0.1A increments every 3 seconds. The voltage measurements are taken through the DAQ system 0.1s after the current increase, to allow time to equilibrate. The heat flux is calculated by using the equation

$$q'' = (I\,V) / (P\,L) \qquad (1)$$

where I is the current input, V is the measured potential drop, P is the perimeter of the cross section of the wire/ribbon, and L is the length of the Nichrome between the voltage sense wires (~40mm). Ohm's law (V=I.R) is used to find the temperature of the Nichrome ribbon wire, T_w, by obtaining the resistance R of the ribbon and then using a temperature-resistance calibration curve, as discussed further later. The pool boiling curve, heat flux versus wall superheat ($T_w - T_{sat}$), is then generated with the acquired data and comparisons are made among the various heater geometries and nanoparticle concentrations. Deposition thickness was measured with calipers. Additionally, visualization of the pool boiling experiments was implemented with a high-speed digital camera (Canon Rebel XT) to aid in conceptual understanding and bubble and glowing length measurements.

Experimental studies of DI water pool boiling were done on several sizes of Nichrome cylindrical wires and rectangular ribbons to find out the impact of shape on the boiling heat transfer behavior. Table I shows the types of heaters used and the convective surface area based on an average length of 40mm for each heater.

Calibration

The temperature-resistance calibration curve (Figure 2) is given as a resistance factor of the temperature by the manufacturer [21]. In the low temperature region the

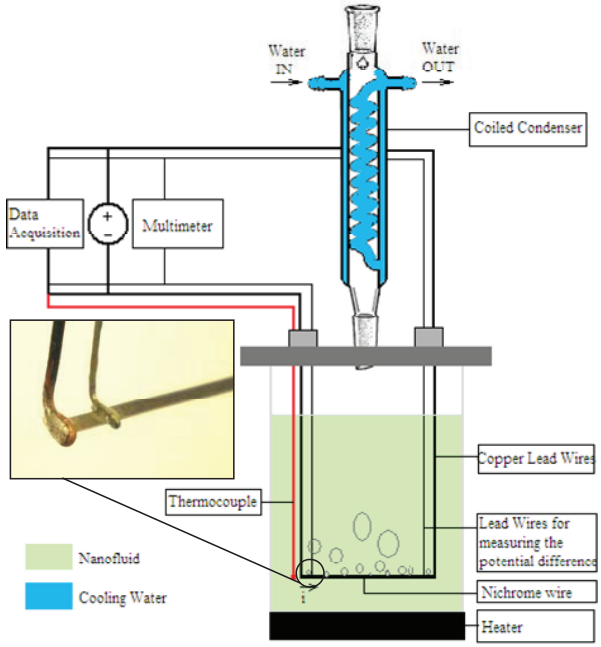

Figure 1 Experimental setup.

TABLE I. CYLINDRICAL WIRES AND RECTANGULAR RIBBONS USED IN EXPERIMENTS AND RESPECTIVE SURFACE AREA

Size Wire/Ribbon	Surface Area [mm^2]
0.32mm Diameter Wire	40.22
0.4 x 0.127mm Ribbon	41.91
0.4mm Diameter Wire	50.75
0.79 x 0.127mm Ribbon	73.66
1.59 x 0.127mm Ribbon	137.16
2.38 x 0.127mm Ribbon	200.66

temperature was seen to be over-predicted for the present experiments; therefore, for the range of 100°C to 150°C, an in situ calibration was done as described in [20] and the resulting correlation can be seen in Figure 2 inset.

Uncertainty in the heat flux calculations can be attributed to instrument errors, random errors and inherent fluctuations in boiling heat transfer and will be represented by error bars in the calculated values of CHF and BHF. Additionally, in nanofluid experiments, inherent small variation of the amount of deposition on the wire causes deviation in heat flux values.

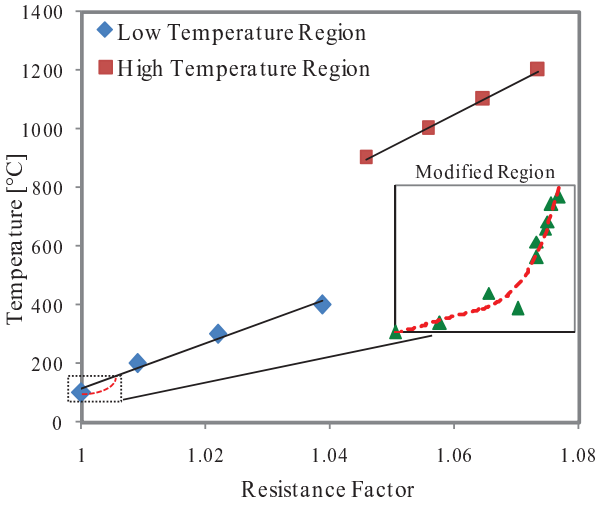

Figure 2 Temperature-resistance calibration with modified region (inset).

Nanofluid Characterization

The nanoparticles obtained are Alfa Aesar® colloidal dispersion of silicon(IV) oxide at 15% concentration in water with 0.83% sodium oxide concentration for stabilization. The initial average particle size is 10nm. Surface tension was measured using calibrated SITA DynoTester® bubble pressure tensiometer. The uncertainty in the measurements are attributed to instrument errors in accuracy and repeatability and are calcluated to be ±1mN/m. The nanofluid pH was measured with a calibrated pH Acorn® 5 Series meter with total instrument error contained within ±0.01 pH. Good mixing and dispersion of the nanoparticles were achieved by 30 minutes magnetic stirring followed by 30 minutes ultrasonic processing (Cole-Parmer®) of each sample. Viscosity measurements were taken with a Brookfield rotational viscometer after mixing and sonicating.

RESULTS AND DISCUSSION

Effect of Nanoparticle Concentration on pH, Viscosity, and Surface Tension

Properties of the nanofluid were measured to gain an understanding of possible influences on the heat transfer behavior of various nanoparticle concentration. Surface tension results are shown in Figure 3 for various particle concentration. The measurements only slightly deviate and are within the uncertainty limits of ±0.01 (ratio); therefore, this suggests that there is a minimal change in surface tension due to the presence of nanoparticles and should have a negligible effect on the heat transfer behavior. Measurements taken after the experiment at room temperature show minimal deviation from DI water as well.

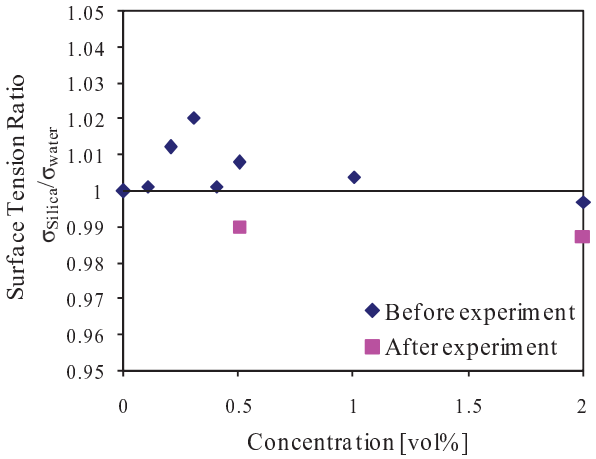

Figure 3 Surface tension of 10nm silica nanofluid at room temperature.

Silica nanofluid with water base is a lyophilic dispersion, which signifies that it acquires stability by hydration of the wetting silica surface [20]. The stability of the nanofluid is an important aspect to consider in regards to the agglomeration and settling of the particles. In order to be stable, nanofluid should be far from its isoelectric point – the pH at which the number of positive and negative particles are equal (unstable nanofluid) [11]. The isoelectric point for silica nanofluid is ~3, and the pH was found to be between 9 and 11 for all concentrations used in this study. Figure 4 shows the pH measurements versus particle concentration, and these results confirm the high negative charge of the silica particles as well as the stability of the nanofluid. Experimental observations suggest no agglomeration or settlement before or after the experiment, and the pH before and after the experiment are very similar, with pH after experiment being slightly smaller due to subtraction of particles which deposited on the wire. Silica particles are highly negatively charged, and high pH indicates a large presence of OH^- ions (hydroxide).

We have shown [22] that with minimal or no nanoparticle deposition on the wire, there was a 50% CHF enhancement which can be attributed solely to the nanoparticle suspension. Silica nanofluid is intrinsically a lyophilic dispersion, and it is thought to be more wettable than pure water due to the hydration layer of the silica particle. The adsorption of water molecules by the silica particle causes the formation of the hydration layer around the particle. The high pH indicates a high concentration of hydroxyl ions and a high charge density (large particle-particle repulsion) [23]. In addition, it also indicates a relatively high amount of hydration of the aqueous silica by way of silanol groups rising from the silica surface. Wen [24] states that nanofluids could exhibit improved spreading and wetting capability in the microlayers underneath growing bubbles causing higher microlayer evaporation. This is inferred from the long-range (a few nanoparticle diameters), structural disjoining pressure theory [25], which postulates that the structural ordering of nanoparticles in very small spaces, i.e., microlayers, creates an oscillatory excess pressure in the thin film which enhances spreadability of the nanofluid on a surface. Figure 4 displays a significant increase in pH (~9) for a relatively small volume fraction of silica particles (0.1vol%). Thus, it is surmised that the enhanced wettability of the working nanofluid due to the hydration layer (high pH) and structural ordering of particles in the microlayer (enhanced spreadability/wettability) have a combined effect of delaying the dryout of the surface and hence increasing the CHF.

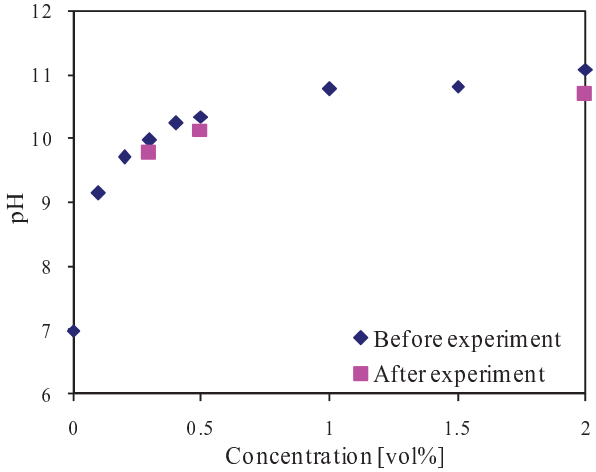

Figure 4 pH of 10nm silica nanofluid at room temperature.

Viscosity measurements, taken after mixing and sonication, are shown in Figure 5 and depict a significant increase in viscosity for higher concentrations of nanoparticle, up to ~40% increase of DI water for 2vol% concentration. At lower concentrations of up to 0.5vol%, the increase in viscosity is less than 15%. Viscosity at higher concentrations rise much more steeply by ~40% and may affect further enhancement of CHF as we will see later.

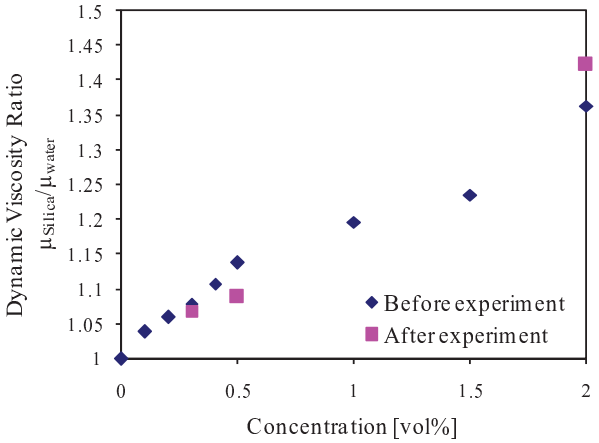

Figure 5 Dynamic viscosity of 10nm silica nanofluid at room temperature.

Effect of Heater Geometry in DI Water on CHF

Figure 6 graphically shows the results of CHF and BHF for different size wires and ribbons for pool boiling experiments in DI water. Error bars represent the standard deviation based on 4 runs for each size. The results show a general decreasing trend of the CHF with increasing convective surface area. It can be noted that the CHF's of each of the cylindrical wires are clearly higher than all of the ribbons. Specifically, for a wire and ribbon of similar surface area, the wire has a CHF increase of 25% over the ribbon. This result suggests a possible dependence of CHF on cross-sectional shape. Also, considering the smallest and largest ribbons used, for an 80% reduction in surface area, the data shows a 28% increase in CHF. These results are in agreement with the established correlations and data of q_{max} dependence on characteristic length for small heaters [26] [27]. In addition, BHF is also depicted on the graph, and it also exhibits a decreasing trend with increasing surface area.

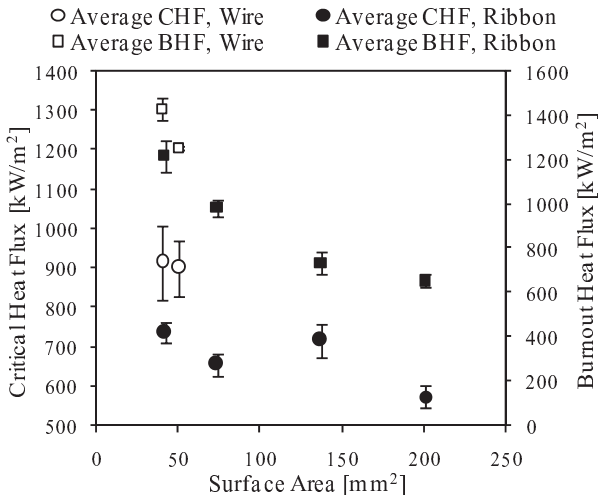

Figure 6 CHF and BHF dependency on heater size and geometry: Experiments in DI water.

Effect of Nanoparticle on Thermal Transport

A notable observation in this study was the deposition of nanoparticles on the boiling surface for all concentrations. This porous deposited layer is formed by ionic attraction forces between the negatively-charged silica particles and the electricity generated through the metal ribbon [20]. In addition, the hydrodynamics of the boiling process could also contribute to the formation of the deposition. It is postulated that microlayer evaporation with subsequent settlement of the nanoparticles contained in it could be the mechanism which forms the porous layer [11].

The flow visualization in Figure 7 shows a comparison of 3 different nanoparticle concentrations and also pure DI water (columns). For each concentration, a progression of heat fluxes (rows) are shown, with the last picture in each sequence representing the moment just before burnout. A comparison of these picture frames shows that while the ribbon in water burns out around 1000kW/m^2, the ribbons in the nanofluid have an extended life. A feature that is noticeable in the early nucleate boiling regime is the presence of small bubbles and an increased bubble number density as concentration increases. This result can be attributed to the increased porosity and higher nucleation site density of the porous layer, rendering a smaller bubble departure radius. It was shown in another study [9] that a direct result of the porous layer was higher nucleation site density. There is evidence in our flow visualization that external vaporization and microconvection due to increased active nucleation sites are the cause for enhancement, as noted by [9].

Another feature that is apparent in the flow visualization is the amount of glowing present, or the glowing length. For pure DI water, the entire ribbon glows after reaching CHF and subsequently breaks. For relatively small concentration of nanofluid, the glowing length is small (only a few millimeters), while it is longer for higher concentrations. The hydrodynamic implication of this is that for small particle concentration (thin porous layer), the moment there is a local dryout of the surface, the temperature increases suddenly under the imposed high heat flux. In this case, the ribbon immediately burns out at that local hot spot, as contrasted by the gradual local to global dryout for higher concentrations (~1.5vol%), as evidenced by the longer glowing length. The sudden burnout can be explained by the hot/dry spot theory proposed by Theofanous et al. [2]. DNB occurs when the evaporation recoil force overcomes the surface tension force which acts to rewet the surface. A dry spot that has developed at high heat flux can be reversed by subsequent rewetting. The increased wettability of the nanoparticle-coated surface causes a delay in the onset of CHF condition, and when it does occur there is a quick burnout of the ribbon. Whereas, for higher concentrations, adverse effects in heat transfer from the heater surface (discussed later) are manifested in the longer glowing length of the ribbon.

There is clearly an overall CHF enhancement for all concentrations measured. In the high heat flux region (slugs and columns regime), it can be seen that the vapor bubbles are relatively large and non-uniformly shaped (Figure 7). These vapor bubbles behave like those of the mushroom vapor bubble theory [3], with feeder jets supplying large amounts of vapor to the mushroom bubble and hence extending heat flux range of the heater.

In the present pool boiling experiments, a 250% to 300% enhancement in CHF has been found for silica nanoparticle concentrations less than 0.5vol% (Figure 8). As Figure 8 shows, the CHF versus particle concentration curve exhibits a non-monotonic behavior, with maximum CHF enhancement occuring between 0.2vol% and 0.4vol%. As concentration is increased further, the CHF decreases and apparently settles to a nominal value. A similar behavior is also seen for BHF versus concentration (Figure 9); maximum BHF enhancement of ~180% is observed between concentrations 0.2vol% to 0.4vol% and subsequently decreases with further increase of concentration. A concurrent event is found in Figure 10, where representative pool boiling curves for each concentration show an increasing wall superheat as concentration increases. This feature is highlighted in Figure 10b with the representative pool boiling curves graphed on a linear plot up to CHF. An

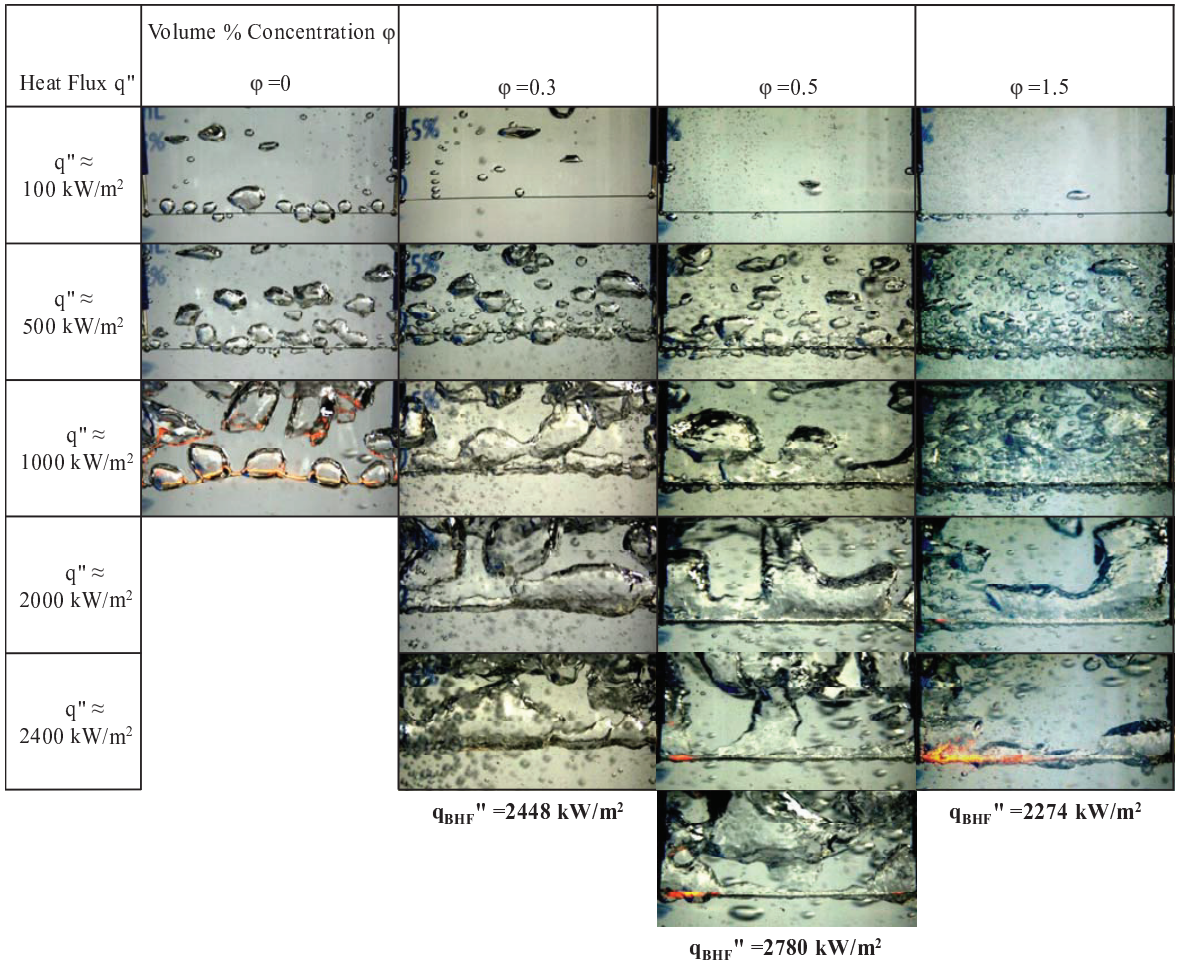

Figure 7 Flow visualization of the pool boiling phenomenon: Particle concentration comparison at various heat fluxes.

investigation of why the superheat at CHF increases in the high heat flux range will illuminate several mechanisms that influence the heat transfer behavior of nanofluids.

The general increasing trend of deposition height with increasing particle concentration can be seen in Figure 11. After a nominal amount of deposition on the bare wire up to 0.5vol%, the deposition level increases rapidly from 0.5vol% to 2vol%. As indicated by [11], the porous surface is more wettable compared to clean surfaces, thus enhancing the cooling effect in the high heat flux range. It can be seen in Figure 12 that for relatively small concentration (~0.1vol%), the wall superheat at the critical heat flux condition has not changed significantly with respect to pool boiling in pure water. However, the CHF wall superheat continues to increase with increasing concentration. The experimental results suggest that the increasing thickness of the porous layer increases the electrical resistance of the circuit, the dependency of which is depicted in Figure 11. In Figure 12 the general increasing trend of wall superheat at CHF with particle concentration can be seen, as well as the resistance ratio from which the temperature was calculated via the resistance-temperature correlation. The electrical resistivity of silica is $>10^{12}$ Ωm, which is significantly larger than that of Nichrome ($\rho = 1.08*10^{-6}$ Ωm); therefore, when the deposition coating thickness increases, the resistance quickly increases, which inherently increases the superheat (Figure 12). The increasing superheat along with the decreasing heat transfer from the heater surface cause the metal to retain more heat, raising its temperature significantly more compared with lower concentrations. Physical evidence of the wall superheat increase at CHF with increasing particle concentration is observed in the present study as increasing glowing length at CHF for increasing concentrations (Figure 7). Therefore, it appears that the competing mechanism for CHF/BHF as concentration increases is enhanced wettability versus a thermal insulation coating effect. A discussion of the hydrodynamic implications of the thermal insulation coating follows.

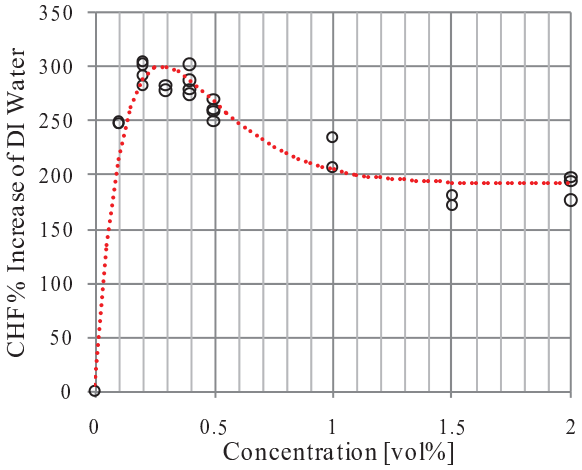

Figure 8 CHF % increase of DI water versus concentration 10nm silica, 0.79mm x 0.127mm ribbon.

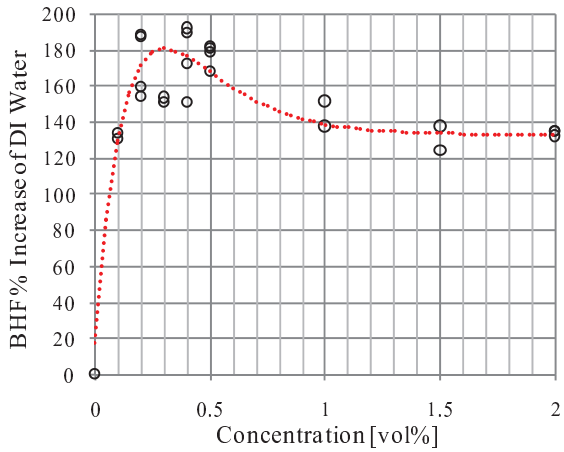

Figure 9 BHF % increase of DI water versus concentration of 10nm silica, 0.79mm x 0.127mm ribbon.

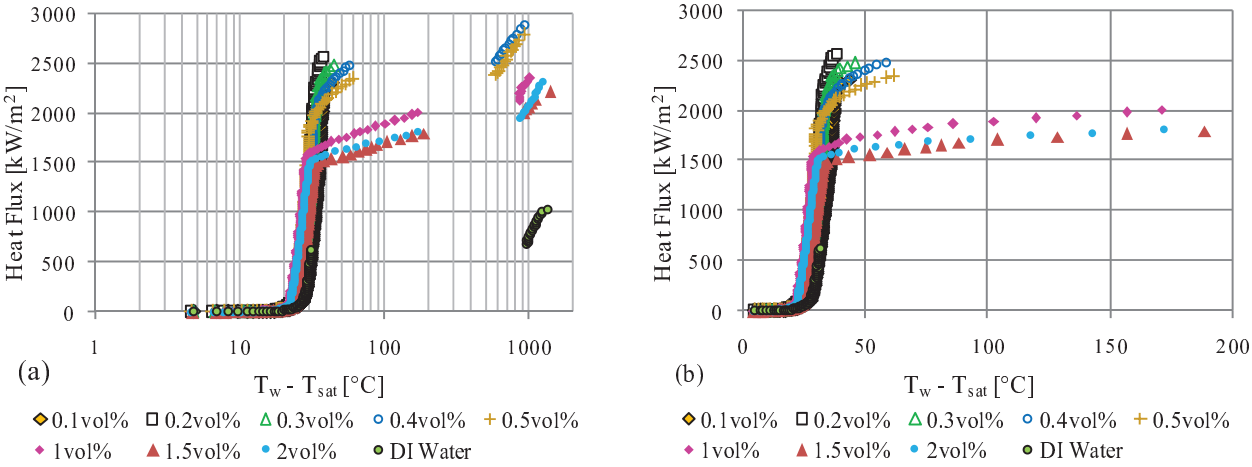

Figure 10 Pool boiling curves for different concentration 10nm silica, 0.79mm x 0.127mm ribbon, a) semilog plot, b) linear plot.

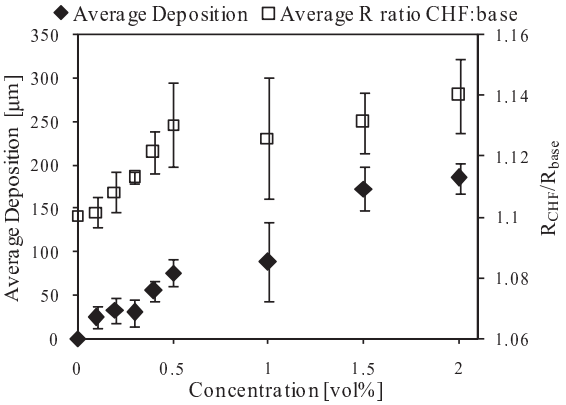

Figure 11 Average silica deposition height versus particle concentration.

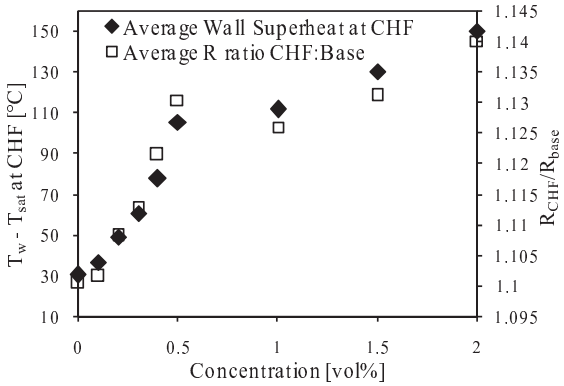

Figure 12 Wall superheat and resistance ratio at CHF location versus concentration.

It may be conjectured that because of the thicker layer on the ribbon, less amount of liquid can reach the sublayers and ultimately the metal surface. Surface characterization experiments done by Kim et al. [14] showed that the type of working fluid also has an effect on capillary wicking in addition to the surface coating itself. They postulate that boiling of nanofluid on a nanoparticle-coated surface could in fact cause clogging of micro-flow-passes due to the suspended nanoparticles. It can be inferred that as particle concentration of the nanofluid increases, the effect of capillary wicking diminishes since there are increasing amounts of suspended particles. Alternatively, it has been suggested that the CHF reaches a plateau for certain critical value of coating thickness [28]. Thome [29] notes that the coating thickness should be maintained thinner than a stipulated value in order to avoid an additional thermal resistance by the particles and entrapped vapor. As particle concentration increases, the contact angle gradually increases [11]. In the present study it was found that wall superheat at CHF increases rapidly to 0.5vol% (Figure 12), and although the superheat continues to increase at all concentrations, the slope is shallow after 0.5vol%, possibly suggesting that the nucleation site density at high heat flux levels starts decreasing beyond 0.5vol%. Therefore, it may be concluded that the combined effect of increasing contact angle (reduced enhancement of wettability), reduced effect of capillary wicking, reduction of nucleation sites, increasing viscosity, and the increasing of thermal resistance contributes to the effective decrease of CHF as particle concentration increases (the roll-over in Figure 8).

CONCLUSIONS

This study has shown a maximum CHF enhancement of 250% to 300% for nanosilica pool boiling for particle concentrations less than 0.5vol%. The relationship of CHF with respect to concentration has been found to be non-monotonic with a peak around 0.2vol% to 0.4vol%. Deposition was observed for all concentrations with a general upward trend. High heat transfer through interagglomerate pores and the highly wettable nature of the nanosilica are thought to be the main factors in CHF enhancement, with declining effect as deposition increases, lending itself to a detrimental thermal resistance effect. Lastly, it was found that pure water pool boiling CHF and BHF decreases with increasing surface area.

REFERENCES

[1] Zuber, N., Hydrodynamic aspects of boiling heat transfer, *AEC Report AECU-4439*, June 1959.

[2] Theofanous, T.G., Dinh, T.N., Tu, J.P., and Dinh, A.T., The boiling crisis phenomenon: Part II: dryout dynamics and burnout, *Exp. Therm. Fluid Sci.*, vol. 26, Aug. 2002, pp. 793–810.

[3] Haramura, Y., and Katto, Y., A new hydrodynamic model of the critical heat flux, applicable widely to both pool and forced convective boiling on submerged bodies in saturated liquids, *Int. J. Heat Mass Transfer*, vol. 26, 1983, pp. 389–399.

[4] Vassallo, P., Kumar, R., and D'Amico, S., Pool boiling heat transfer experiments in silica–water nano-fluids, *Int. J. Heat Mass Transfer*, vol. 47, Jan. 2004, pp. 407–411.

[5] Milanova, D., and Kumar, R., Role of ions in pool boiling heat transfer of pure and silica nanofluids, *Appl. Phys. Lett.*, vol. 87, 2005, pp. 233107-1–233107-3.

[6] Kim, H., Kim, J., and Kim, M.H., Effect of nanoparticles on CHF enhancement in pool boiling of nano-fluids, *Int. J. Heat Mass Transfer*, vol. 49, Dec. 2006, pp. 5070-5074.

[7] You, S.M., Kim, J.H., and Kim, K.H., Effect of nanoparticles on critical heat flux of water in pool boiling heat transfer, *Appl. Phys. Lett.*, vol. 83, Oct. 2003, pp. 3374–3376.

[8] Bang, I.C., and Chang, S. H., Boiling heat transfer performance and phenomena of Al2O3–water nano-fluids from a plain surface in a pool, *Int. J. Heat Mass Transfer*, vol. 48, June 2005, pp. 2407–2419.

[9] Chang, J.Y., and You, S.M., Enhanced boiling heat transfer from microporous surfaces: effects of a coating composition and method, *Int. J. Heat Mass Transfer*, vol. 40, Dec. 1997, pp. 4449-4460.

[10] Wen, D., and Ding, Y., Experimental investigation into the pool boiling heat transfer of aqueous based gamma alumina nanofluids, *J. Nanoparticle Res.*, vol. 7, June 2005, pp. 265–274.

[11] Kim, S.J., Bang, I.C., Buongiorno, J., and Hu, L.W., Surface wettability change during pool boiling of nanofluids and its effect on critical heat flux, *Int. J. Heat Mass Transfer*, vol. 50, Sept. 2007, pp. 4105–4116.

[12] Das, S.K., Putra, N., and Roetzel, W., Pool boiling characteristics of nano-fluids, *Int. J. Heat Mass Transfer*, vol. 46, Feb. 2003, pp. 851–862.

[13] Wenzel, R.N., Surface roughness and contact angle, *J. Phys. Colloid Chem.*, vol. 53, 1949, pp. 1466–1467.

[14] Kim, H.D., Kim, J., and Kim, M.H., Experimental studies on CHF characteristics of nano-fluids at pool boiling, *Int. J. Multiphase Flow*, vol. 33, July 2007, pp. 691–706.

[15] Liaw, S.P., Dhir, V.K., Effect of surface wettability on transition boiling heat transfer from a vertical surface, *Proceedings of the Eighth International Heat Transfer Conference*, San Francisco, CA, vol. 4, 1986, pp. 2031–2036.

[16] Coursey, J.S., and Kim, J., Nanofluid boiling: The effect of surface wettability, *Int. J. Heat Fluid Flow*, vol. 29, Dec. 2008, pp. 1577–1585.

[17] Liu, Z., and Liao, L., Sorption and agglutination phenomenon of nanofluids on a plain heating surface during pool boiling, *Int. J. Heat Mass Transfer*, vol. 51, May 2008, pp. 2593–2602.

[18] Kim, H.D., and Kim, M.H., Effect of nanoparticle deposition on capillary wicking that influences the critical heat flux in nanofluids, *Appl. Phys. Lett.*, vol. 91, July 2007, pp. 014104-1–014104-3.

[19] Liter, S.G., and Kaviany, M., Pool-boiling CHF enhancement by modulated porous-layer coating: theory and experiment, *Int. J. Heat Mass Transfer*, vol. 44, Nov. 2001, pp. 4287–4311.

[20] Kumar, R., and Milanova, D., Dispersion and Surface Characteristics of Nano-Oxide Suspensions, *Ann. N.Y. Acad. Sci.*, vol. 1161, 2009, pp.472-483.

[21] Hyndman Industrial Products, Inc., Resistance wire heating data, www.resistancewire.com, 2009.

[22] Milanova, D., and Kumar, R., Heat transfer behavior of silica nanoparticles in pool boiling experiment, *J. Heat Transfer*, vol. 130, April 2008, pp. 042401-1–042401-6.

[23] Bergna, H.E., and Roberts, W.O., Colloidal silica: fundamentals and applications, Boca Raton, FL: *CRC Taylor & Francis*, 2006, pp. 139.

[24] Wen, D., Mechanisms of thermal nanofluids on enhanced critical heat flux (CHF), *Int. J. Heat Mass Transfer*, vol. 51, Sept. 2008, pp. 4958-4965.

[25] Wasan, D., and Nikolov, A., Spreading of nanofluids on solids, *Nature*, vol. 423, 2003, pp. 156–159.
[26] Lienhard, J.H., A heat transfer textbook, Englewood Cliffs, N.J.: *Prentice-Hall*, 1987, pp. 404–438.
[27] Gjerkes, H., and Golobic, I., Pool boiling CHF on a laser heated thin plate, *Int. J. Heat Mass Transfer*, vol. 43, June 2000, pp. 1999–2008.
[28] Hwang, G.-S., and Kaviany, M., Critical heat flux in thin, uniform particle coatings, *Int. J. Heat Mass Transfer*, vol. 49, Mar. 2006, pp. 844–849.
[29] Thome, J.R., Enhanced Boiling Heat Transfer, *Hemisphere*, New York, 1990.